International Journal of Extreme Manufacturing

TOPICAL REVIEW • OPEN ACCESS

Atomic layer deposition in advanced display technologies: from photoluminescence to encapsulation

To cite this article: Rong Chen *et al* 2024 *Int. J. Extrem. Manuf.* **6** 022003

View the article online for updates and enhancements.

You may also like

- Luminescent materials for modern light sources
Pavel P. Zak, Viktoriya A. Lapina, Tatyana A. Pavich et al.

- Luminous properties of recycling luminous materials $SrAl_2O_4:Eu^{2+}, Dy^{3+}$ based on luminous polyester fabric
Yanan Zhu, Qincen Yu, Liubin Zheng et al.

- Influence of fluorescent pigments on the spectral characteristics of luminous coated fabrics
Jing Li, Yanan Zhu and Mingqiao Ge

This content was downloaded from IP address 220.166.33.21 on 08/01/2024 at 00:44

OPEN ACCESS
IOP Publishing | IMMT
International Journal of Extreme Manufacturing
Int. J. Extrem. Manuf. 6 (2024) 022003 (18pp) https://doi.org/10.1088/2631-7990/ad15f5

Topical Review

Atomic layer deposition in advanced display technologies: from photoluminescence to encapsulation

Rong Chen[1,*], Kun Cao[1], Yanwei Wen[2], Fan Yang[1], Jian Wang[1], Xiao Liu[1] and Bin Shan[2]

[1] State Key Laboratory of Intelligent Manufacturing Equipment and Technology, School of Mechanical Science and Engineering, Huazhong University of Science and Technology, Wuhan 430074, Hubei, People's Republic of China
[2] State Key Laboratory of Materials Processing and Die & Mould Technology, School of Materials Science and Engineering, Huazhong University of Science and Technology, Wuhan 430074, Hubei, People's Republic of China

E-mail: rongchen@mail.hust.edu.cn

Received 16 June 2023, revised 7 August 2023
Accepted for publication 13 December 2023
Published 5 January 2024

Abstract

Driven by the growing demand for next-generation displays, the development of advanced luminescent materials with exceptional photoelectric properties is rapidly accelerating, with such materials including quantum dots and phosphors, etc. Nevertheless, the primary challenge preventing the practical application of these luminescent materials lies in meeting the required durability standards. Atomic layer deposition (ALD) has, therefore, been employed to stabilize luminescent materials, and as a result, flexible display devices have been fabricated through material modification, surface and interface engineering, encapsulation, cross-scale manufacturing, and simulations. In addition, the appropriate equipment has been developed for both spatial ALD and fluidized ALD to satisfy the low-cost, high-efficiency, and high-reliability manufacturing requirements. This strategic approach establishes the groundwork for the development of ultra-stable luminescent materials, highly efficient light-emitting diodes (LEDs), and thin-film packaging. Ultimately, this significantly enhances their potential applicability in LED illumination and backlighted displays, marking a notable advancement in the display industry.

Keywords: atomic layer deposition, display, luminescent, encapsulation

[*] Author to whom any correspondence should be addressed.

Original content from this work may be used under the terms of the Creative Commons Attribution 4.0 licence. Any further distribution of this work must maintain attribution to the author(s) and the title of the work, journal citation and DOI.

© 2024 The Author(s). Published by IOP Publishing Ltd on behalf of the IMMT

1. Introduction

Rapid developments in the field of advanced displays have led to accelerated progress in smartphones, projectors, televisions, medical images, and augmented reality/virtual reality devices [1, 2]. However, advanced display technologies require high device flexibility, low power consumption, high stability, and high resolution. Although advances in organic light-emitting diodes (OLEDs) and quantum dot light-emitting diodes (QLEDs) have enabled the development of flexible mobile phones and curved televisions, their short lifespans and relatively rapid aging remain unresolved. The further evolution of these technologies, therefore, demands the development of new luminescent materials that meet the stringent standards of low toxicity and excellent stability, while also being cost-effective [3–5]. Unfortunately, the intrinsic instability issues associated with these newly developed luminescent materials can lead to a degradation in the luminescence efficiency over prolonged operations [6–8]. Therefore, improving both the luminescent performances and the durability of these materials requires comprehensive multi-scale fabrication strategies.

Currently, strategies used to improve the performances of luminescent materials mainly involve crystal structure modification, composition regulation, and surface modification. Doping is also a practical and effective means for tuning the crystal lattices and improving the stabilities of luminescent quantum dot (QD) materials [9, 10]. Surface coating is another effective method for passivating surface defects and functionalizing materials [11, 12]. More specifically, surface coating with organic or inorganic materials improves the resistance of luminous materials to aggregation, infiltration, high-temperature degradation, and corrosion. Commonly used coating technologies include wet methods (colloidal coating) and dry methods (chemical vapor deposition (CVD) and physical vapor deposition (PVD)). In addition, gas-phase thin-film fabrication methods include PVD, CVD, plasma-enhanced CVD (PECVD), and the atomic layer deposition (ALD) of an inorganic layer. Solution-based methods include spin-coating and inkjet printing. Unfortunately, the polymer layers fabricated using these methods are known to exhibit poor gas-diffusion barrier properties owing to their high polymeric porosities [13–15]. However, ALD is a relatively low temperature process that provides a high film quality for the preparation of luminescent materials and their corresponding devices [16–18]. To date, ALD has been used to coat the surfaces of nitride red phosphors and QDs with nano-thin films, while precisely controlling the coating thickness by changing the ALD cycles and other process parameters. This has led to improved luminescence performances, thermal stabilities, and durabilities, among other desirable properties [16, 19].

The ALD technique was first described by Sanders, wherein it was employed for the deposition of ZnS [20]. In addition, although atomic layer epitaxy was first referred to by Suntola and Antson in 1977, it was later discovered that in most cases, the thin films produced under these conditions were not grown epitaxially, but rather underwent a self-limiting reaction, which gradually led to the evolution of ALD. The early applications of ALD were primarily focused on microelectronics and nanotechnology; however, in the past few decades, ALD has been extensively used in the production of semiconductors due to its ability to grow high-quality dielectrics and semiconductors on different substrates (e.g. porous, organic, and high-aspect-ratio substrates) for use in solar cells, photodetectors, and other electronic devices [21, 22]. Characterized by its ability to control the atomic thickness of the deposited film, ALD is also considered desirable due to its relatively mild process conditions, excellent conformality, and defect-free uniformity. Such properties render it particularly advantageous for the surface regulation and coating of QDs, phosphors, and organic luminescent materials, resulting in enhanced stabilities, optimized carrier mobilities, and regulated interface energy levels.

ALD also serves as a powerful method for generating thin-film encapsulations (TFEs) in flexible electronics owing to its pinhole-free advantages, excellent conformality, and precise nanoscale thickness control over large areas [23–25]. However, conventional temporal ALD processes suffer from slow film deposition speeds, rendering them unsuitable for use in mass production [17]. As depicted in figure 1, ALD has been explored for use in flexible display applications ranging from material modification to encapsulation. This has led to the development of multi-scale manufacturing strategies for stabilizing flexible displays, with the aim of satisfying the manufacturing requirements of flexible QD display devices. In addition, ALD has been used to precisely passivate surface defects at the atomic level and effectively shield luminescent materials from external environmental factors. The ongoing development of ALD equipment is also necessary to ensure that conformal deposition is achieved on nanoparticles, high-aspect-ratio nanostructures, and large-area substrates.

2. Multi-scale ALD stabilization strategies

In recent decades, ALD has played a crucial role in enhancing material properties and device performances. As shown in figure 2, the development of ALD has significantly impacted various applications, including luminescent materials for use in advanced displays, functional micro/nano-LED and QLED layers, and thin-film transistor (TFT) displays, and for the encapsulation of displays.

Within the context of luminescent materials, the use of ALD to prepare surface coatings and achieve defect passivation leads to an improved device efficiency, in addition to enhancing resistances to humidity and high temperatures. The suitability of the ALD procedure has also been demonstrated in optimizing the radiative recombination of emission layers (EMLs) and the conductivity of electron transport layers (ETLs), while also blocking ion diffusion in indium tin oxide (ITO), suppressing exciton quenching in the hole transport layers (HTLs), and promoting the dual fabrication of ETLs for use in LED displays. In addition, the encapsulation of OLED

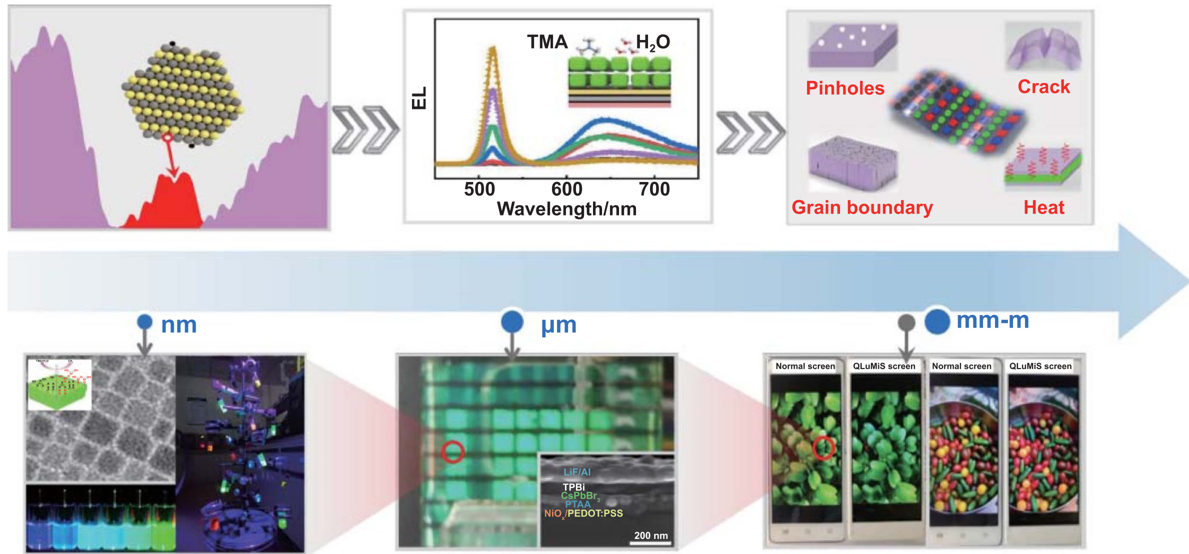

Figure 1. Multi-scale manufacturing scheme for the production of displays and luminescence materials, and for display encapsulation. Reprinted with permission from [26]. Copyright (2021) American Chemical Society. Reprinted with permission from [27]. Copyright (2020) American Chemical Society. [28] John Wiley & Sons.© 2020 WILEY-VCH Verlag GmbH & Co. KGaA, Weinheim. Reprinted from [29], with the permission of AIP Publishing. Reprinted with permission from [30]. Copyright (2021) American Chemical Society.

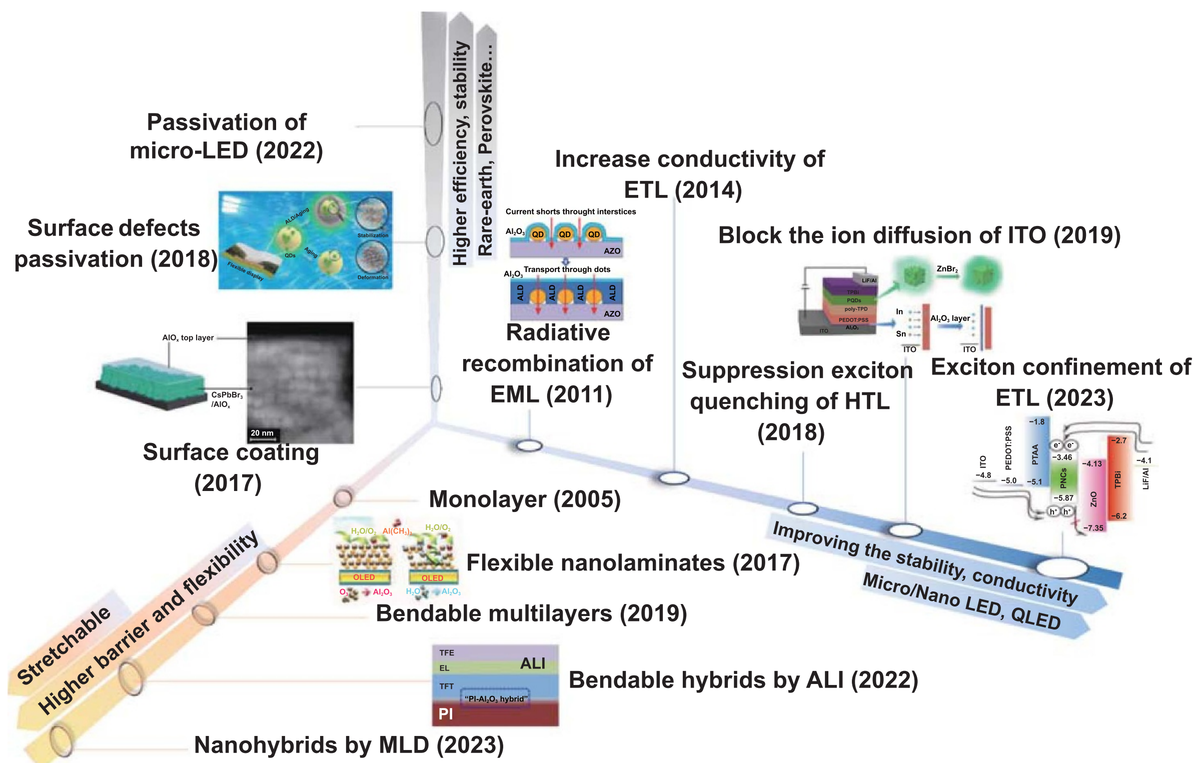

Figure 2. The development of atomic layer deposition (ALD) across diverse applications, spanning luminescent materials for advanced displays. [31] John Wiley & Sons.© 2017 Wiley-VCH Verlag GmbH & Co. KGaA, Weinheim. Reprinted with permission from [32]. Copyright (2018) American Chemical Society. [33] John Wiley & Sons. Copyright © 2011 WILEY-VCH Verlag GmbH & Co. KGaA, Weinheim. Reprinted with permission from [26]. Copyright (2021) American Chemical Society. Reproduced from [34]. © IOP Publishing Ltd All rights reserved. Reprinted with permission from [35]. Copyright (2013) American Chemical Society. Reproduced from [36]. CC BY 4.0.

displays using ALD led to a significantly higher barrier and an improved device flexibility. It should be noted here that encapsulated structures can include monolayers, nanolaminates, organic/inorganic multilayers, and hybrid films. Furthermore, ALD film encapsulation methods also encompass the plasma enhanced ALD (PEALD), atomic layer infiltration (ALI),

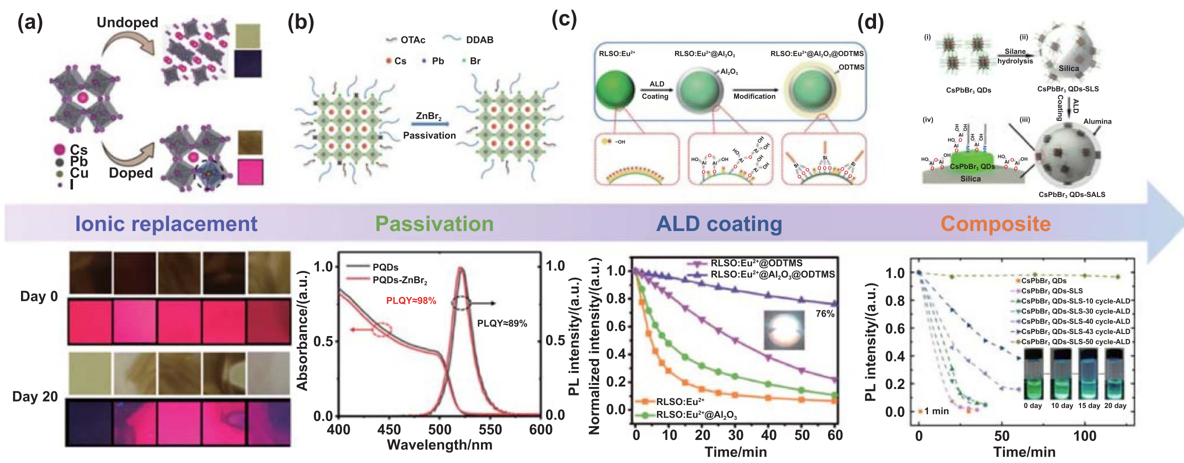

Figure 3. Schematic diagram outlining the strategies employed to improve the stabilities of luminescent materials: (a) ionic replacement. Reprinted with permission from [39]. Copyright (2021) American Chemical Society. (b) Surface passivation. [42] John Wiley & Sons.© 2020 Wiley-VCH Verlag GmbH & Co. KGaA, Weinheim. (c) ALD coating. Reprinted with permission from [32]. Copyright (2018) American Chemical Society. And (d) composite structures. Reprinted with permission from [26]. Copyright (2021) American Chemical Society.

and plasma enhanced molecular layer deposition (PEMLD) techniques.

2.1. Surface modification on photoluminescence nanocrystals

Under the influence of humidity, heat, light, and other factors, luminescent materials are known to be prone to surface damage, aggregation, and phase deformation, which can lead to serious photoluminescence (PL) quenching [37, 38]. To address such issues, these materials can be stabilized by ALD through surface passivation, coating, and the formation of composite structures.

The crystal structures of luminescent materials are closely related to their properties, and so to tune such properties, the ion doping method is commonly employed. As shown in figure 3(a), B-site ion doping can enhance the phase and thermal stabilities of perovskite nanocrystals, and first-principles calculations suggest that B-site ions with small radii effectively increase the formation energy of the perovskite structure [39]. To passivate surface defects and reduce non-radiative recombination, Lewis acids, trimethylaluminum (TMA), and hydrobromic acid have been used to promote phase transformation from Cs_4PbBr_6 to luminous $CsPbBr_3$ perovskite nanocrystals, while also passivating the luminous nanocrystals *in situ* [40]. As indicated in figure 3(b), an X-type ligand containing Br^- can undergo ligand exchange with the long chain ligand on the surface. The introduction of Br can therefore repair surface halogen defects to remove traps, which are known to induce non-radiative recombination [26, 27]. As a result, the PL quantum yield (PLQY) of the resulting luminescent materials was improved to ~100%. Such repair of the surface halogen defects maintains the integrity of the Pb–Br octahedra to provide highly stable perovskite QDs.

A key application of ALD is the surface coating of luminescent materials. By depositing precise and conformal thin films onto the surfaces of luminescent materials, ALD enhances the light emission efficiency and stability of these materials [31]. Beyond surface passivation, a combination of oxide infiltration and ALD coating has been used to prevent crystal deformation and ligand desorption in luminescent materials. A two-step hybrid passivation strategy was also developed to improve the performances of luminescent materials by surface halogen replenishment, and to enhance their stabilities following ALD coating. It should be noted here that PL quenching during ALD can be minimized by controlling the ligand density on the nanocrystal surface. Indeed, the ALD coating of the material with alumina led to an improved long-term stability, wherein 100% of the original PL value was retained after 48 h of ultraviolet (UV) irradiation. Furthermore, a SiO_2 PEALD method was developed to effectively stabilize luminescent QD materials [41]. This process was conducted at a relatively low temperature (50 °C), preventing damage to the surface ligands or etching of the QDs, and it also preserved the optical performances of the luminescent QD materials. As a result, the SiO_2-coated $CsPbBr_3$ QDs retained 80% of their original PL intensity and demonstrated significantly improved stabilities in the presence of water, light, and heat. As mentioned above, the presence of surface defects can lead to non-radiative recombination, thereby reducing the overall luminous efficiency. However, when ALD is employed, these defects can be effectively passivated, minimizing non-radiative processes and improving the luminescence properties of the resulting materials [32].

The ALD technology has also been extended to form composite structures designed to protect luminescent phosphor materials [42]. As shown in figure 3(c), amorphous Al_2O_3 combined with hydrophobic modification by octadecyltrimethoxysilane (ODTMS) was used to construct the moisture-resistant dual-shelled RLSO:Eu^{2+}@Al_2O_3@ODTMS composite. For this purpose, ALD was initially performed to provide an ultrathin but dense alumina coating on the RLSO:Eu^{2+} surface, and subsequent hydrophobic surface modification was achieved by the introduction of ODTMS.

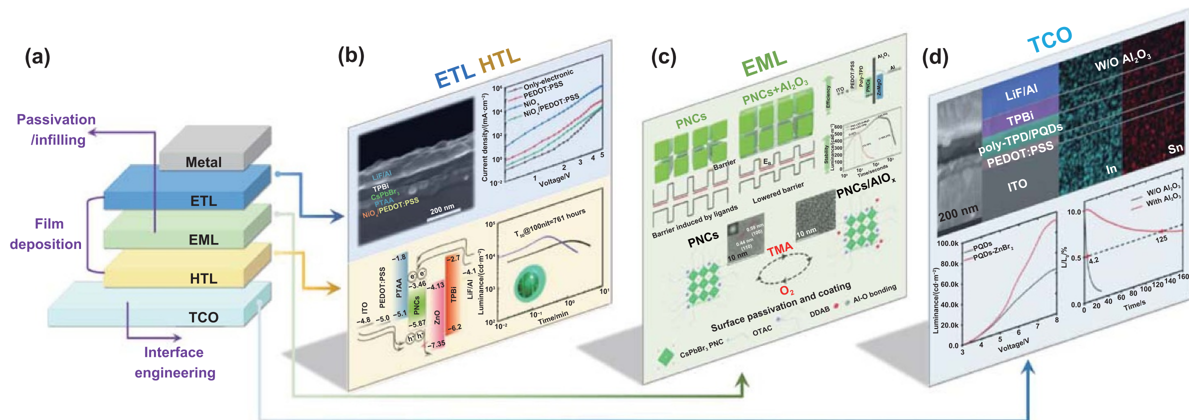

Figure 4. Application of ALD in the fabrication of PQLEDs. (a) Various ALD strategy in the PQLEDs. (b) Film deposition with dual ETL and HIL layers. Reproduced from [34]. © IOP Publishing Ltd. All rights reserved. Reprinted from [29], with the permission of AIP Publishing. (c) Coating and filling of the EML. [47] John Wiley & Sons. © 2020 WILEY-VCH Verlag GmbH & Co. KGaA, Weinheim. Reprinted with permission from [30]. Copyright (2021) American Chemical Society. (d) Interface engineering to block ion diffusion. Reprinted with permission from [26]. Copyright (2021) American Chemical Society.

The resulting phosphors exhibited remarkably improved moisture resistance properties. In addition, the investigation of the photoelectric properties of the fabricated white LED devices indicated that the obtained phosphors are promising candidates for applications in high-power LED backlights. Moreover, as shown in figure 3(d), coatings generated through a combination of ALD and silica composite microspheres have also been developed [32]. More specifically, silicon spheres were subjected to surface passivation and QD coating using the ALD technology to further enhance the stabilities of the luminescent QD materials without damaging the surface ligands or degrading the optical performances [28]. Importantly, upon scaling micro-LEDs down to nanoscale dimensions, surface defects become more pronounced and detrimental to their performances. Thus, ALD clearly offers a precise and controlled method to passivate the surfaces of micro-LEDs, leading to higher luminous efficiencies and improved overall device reliabilities [43]. The future development of ALD is therefore expected to focus on enhancing luminous efficiencies, stabilities, and temperature resistances of luminescent materials based on new materials, such as rare-earth elements, perovskites, and metal–organic frameworks.

2.2. Fabrication of functional layers for QD devices

Although the PLQYs and stabilities of QDs have been improved through surface passivation, the introduction of coatings, and the use of composites, perovskite QLED (PQLED) devices still face significant challenges in terms of solvent erosion, ion migration, carrier transport, and Joule heating during device fabrication and operation. In general, the low optoelectronic efficiencies and short lifetimes of QD optoelectronic devices limit their further applications [16, 44]. To address such issues, ALD has been shown to exhibit great advantages in the preparation and modification of the functional layers of QD-based devices. Li *et al* performed the vapor infiltration of metal oxides into the EMLs of perovskite nanocrystals (PNCs) to yield highly efficient and long-lifetime PNCs LED due to the improved electron–hole capture ability and the imparted functional layer protection [45]. In addition, Kumah *et al* introduced epitaxial oxides onto semiconductors via ALD to prepare new devices and lay the groundwork for the realization of ALD-modified functional layers in optoelectronic devices [22].

The ALD process employed to modify the PQLEDs is shown in figure 4(a), wherein the EML can be modified, functional layers can be fabricated, and the interfaces between the different functional layers in the sandwich-structured PQLEDs can be engineered. As current-derived devices, carrier injection and transport are essential in terms of the light-emitting performances of such devices. Thus, figure 4(b) outlines the process employed to construct ETLs and HTLs via ALD based on a well-controlled thickness. More specifically, a layer of zinc oxide layer is deposited onto 1,3,5-tris(1-phenyl-1*H*-benzimidazol-2-yl)benzene via ALD at low temperatures to form inorganic/organic dual ETLs in the device structure (top inset, figure 4(b)) [34]. As a result, the external quantum efficiency (EQE) of the device was improved significantly due to the enhanced charge transport balance with favorable energy level matching [46]. Moreover, the T_{50} lifetime of the device was increased to 761 h at the initial luminance of 100 nit, which is one of the highest lifetimes reported to date for PQLEDs [34]. In another study, a NiO_x film was deposited on poly(ethylene dioxythiophene):polystyrene sulfonate (PEDOT:PSS) to fabricate an inorganic/organic dual hole injection layer (HIL, bottom inset, figure 4(b)) [29]. The electroluminescence of the resulting fluorescent material indicated that non-radiative recombination was suppressed in the ELT. Thus, due to an improved carrier transport balance and an effective degree of radiative recombination, the EQE of the PQLED increased significantly from 1.5% to 9.7%. These results clearly indicate that ALD modification improves the conductivity and carrier transport balance to produce highly efficient PQLEDs with long lifetimes.

In the context of lighting and displays, the EML is a key component in the PQLED structure due to the fact that carrier recombination and emission occur in this layer. As previously reported, passivation and core–shell coating are common methods that have been employed to improve the light emission properties of QDs. As shown in the top inset of figure 4(c), the application of ALD to modify the electronic properties of the EMLs [30, 47] led to a significantly improved carrier mobility due to the decreased energy barrier between the various QDs [33, 48]. In addition, the coating of nanocrystals with a thin ALD film (nanometer scale) reduced the film resistivity by seven orders of magnitude [49], while the introduction of alumina suppressed excess electron transport to achieve a favorable carrier transport balance and facilitate effective carrier combination [50]. Furthermore, a facile colloidal layer-by-layer deposition of amorphous AlO_x (bottom inset, figure 4(c)) was proposed to improve the water resistance properties of perovskite QDs and suppress ionic mixing of the $CsPbBr_3$ and $CsPbI_3$ QDs under irradiation conditions [30]. It was found that the integrated PQLEDs exhibited significantly improved EQEs with high luminance capabilities due to an optimized band alignment. Moreover, precise control of the ALD process at the atomic scale allows modification of the interfaces between the different functional layers. Such interface modification can remove defects and provide effective protection to the underlying layer of the device structure. As shown in figure 4(c), an ultrathin Al_2O_3 insertion layer can be introduced between the ITO layer and the PEDOT:PSS layer via ALD to increase the maximum luminance [26]. This effect was attributed to the passivation of the Br vacancies on the QD surfaces, which achieves a near-unity PLQY. In addition, the T_{50} lifetime of the device was prolonged by a factor of 30, owing to the suppression of PL quenching upon the introduction of an Al_2O_3 buffer layer. The transmission electron microscopy (TEM) and elemental mapping images of the device cross-sections (figure 4(d)) show that in the presence of Al_2O_3, the diffusion of indium ions from the ITO layer into the PEDOT:PSS layer and the EML is blocked, thereby enhancing the PQLED stability. It was also found that the introduced ultrathin Al_2O_3 layer modified the energy level of the device and achieved a favorable balance of carrier injection, further contributing to a high EQE. Upon the use of ALD to introduce an ITO barrier layer in advanced displays, ion diffusion from the ITO layer was effectively blocked, mitigating device degradation and enhancing its long-term stability [26, 51]. Additionally, ALD enables efficient exciton confinement during dual-ETL fabrication [34], ultimately enhancing the display performance and efficiency.

Overall, the above studies demonstrate that ALD can modify the PQLED in each functional layer to improve the PLQY and device stability. However, the position of the ALD modification should be carefully selected, wherein the introduction of metal oxide layers is favorable to induce energy-level matching between different functional layers. Thus, following suitable modification of the functional layers, an excellent transport balance between the electrons and holes can be achieved. Moreover, the introduced ALD layers can also act as barriers to confine excitons and improve radiative recombination in the EML [34].

2.3. Manufacturing of the rigid and flexible encapsulation layers

Although OLED and QLEDs have recently undergone significant developments [52], OLED and QLED devices and displays remain prone to degradation due to optical aging, the influence of the electric field, and the effects of moisture, oxygen, and external stress [53]. Thus, to improve the long-term stabilities of display devices and promote their industrialization, encapsulation is an indispensable and effective means to protect the devices from moisture presented in the atmosphere. Indeed, the requirements of an encapsulation layer for barrier protection are extremely strict. For example, to produce a QLED with a lifetime $>$10 000 h, the water vapor transmission rate (WVTR) and oxygen transmission rate should not exceed 10^{-6} g m^{-2} d^{-1} and 10^{-5} ml m^{-2} d^{-1}, respectively [54–57]. With the development of high-definition, thin, and flexible display technologies, rigid, flexible, bendable, and stretchable devices can be produced (figure 5). It is therefore necessary to develop serial encapsulation structures to improve the stabilities of display devices during operation.

Compared with traditional glass encapsulation, TFE has emerged as a promising method due to its ability to produce high transparency, ultra-thin, and highly flexible films. Among the various thin film fabrication methods described to date, ALD is capable of depositing ultrathin and pinhole-free inorganic films at the atomic level and at low temperatures ($<$100 °C) [58, 59]. In addition, it allows precise thickness control, high densification, and excellent conformality over large areas owing to the self-limiting nature of the reactions involved.

In terms of rigid OLED device encapsulation, the application of ALD has seen remarkable progress over recent years, achieving increasingly high barrier performances. For example, a monolayer with a relatively low WVTR of 10^{-2} g m^{-2} d^{-1} was fabricated by ALD [60]. In addition, Kim and Kim reported rigid OLED device encapsulation by combining the PECVD and spatial ALD (SALD) methods to fabricate a binary Al_2O_3/SiN_x structure [61]. By drawing metal compound films with reverse stress, the overall residual stress of the encapsulation layer was regulated. Thus, the introduction of the ALD-based nanoscale Al_2O_3 layer was conducive to decoupling the defects in the PECVD-based SiN_x layer, ultimately leading to a lower WVTR in the Al_2O_3/SiN_x barrier film. As shown in figure 5(a), the interface bonding strength between the Al_2O_3/SiN_x encapsulation structure and the OLED is five orders of magnitude higher than that of a single SiN_x thin film under damp heat conditions, which effectively prevents buckling of the encapsulation structure [54].

However, with the rapid development of display devices ranging in flexibility from rigid to extremely flexible, inorganic composite encapsulation films have been unable to simultaneously satisfy the flexibility and barrier property requirements. For example, although nanolaminates fabricated by

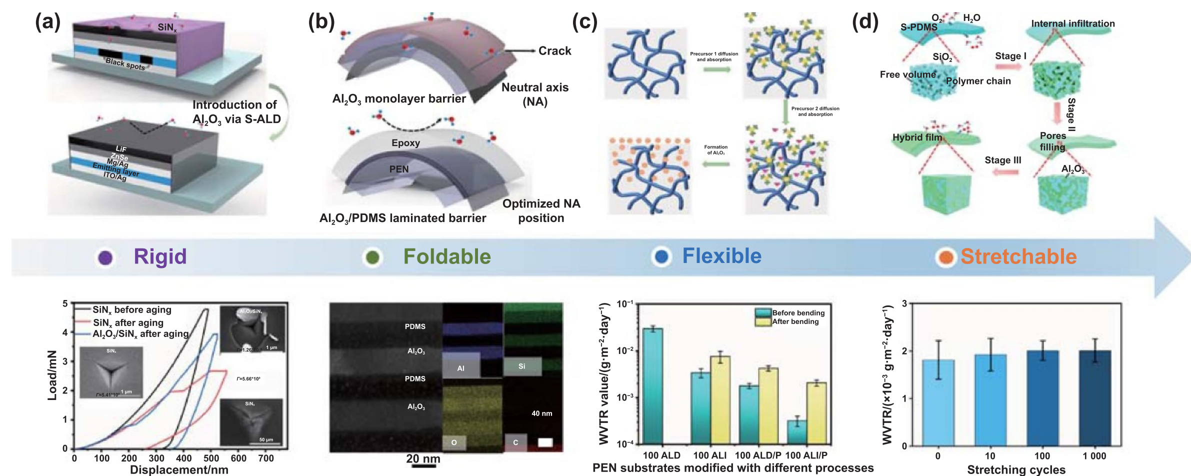

Figure 5. Schematic diagrams outlining encapsulation strategies for improving the stabilities of device materials: (a) rigid materials, Reproduced from [76], with permission from Springer Nature. (b) Foldable materials, [57] John Wiley & Sons. © 2021 Wiley-VCH GmbH. (c) Flexible materials, Reproduced from [66] with permission from the Royal Society of Chemistry. (d) Stretchable materials, [75] John Wiley & Sons.© 2021 Wiley-VCH GmbH.

ALD exhibit excellent barrier properties, their flexibility is limited, because they can only withstand a bending radius of 10 mm [35]. As such, there is an urgent demand for the development of flexible encapsulation films. Although a low WVTR can be achieved by the introduction of an ALD-based barrier film [59, 62], and the flexibility can be improved by the implementation of thin barrier films, the barrier properties of such films have been found to deteriorate by several orders of magnitude after a very short exposure time to damp heat conditions. As an alternative, polymers were considered, which are widely used as substrates in flexible electronics because of their light weight and low cost nature, in addition to their high transparency and good flexibility [63, 64]. In this context, Wilson *et al* and our present research group have examined a number of polymer substrates, including polyethylene naphthalate (PEN) [65], polyethylene terephthalate (PET) [66], and polycarbonate [67], demonstrating that these polymers exhibit almost no barrier ability. Using the ALD approach, our group further integrated the spin-coating process to introduce a nanoscale layer of polydimethylsiloxane (PDMS). As a result, a lower WVTR was achieved ($\sim 10^{-5}$ g m^{-2} d^{-1}) using the PDMS/Al_2O_3 nanolaminates to encapsulate the OLED [66]. The clear interface of the PDMS/Al_2O_3 nano-laminated encapsulation structure is shown in figure 5(b) [57]. Additionally, ALD-based multilayers were developed to give a WVTR of 10^{-5} g m^{-2} d^{-1} and a bending radius of 3 mm [68].

Furthermore, the ALI method is a breakthrough in the preparation of inorganic–organic hybrid structures because of the excellent mechanical stability and barrier properties that it imparts on materials. Using the ALI process, the deposition of Al_2O_3 on a polymer substrate [66] usually involves swelling of the polymeric substrates, infiltration of an organometallic precursor (TMA) into the subsurface, the formation of Al_2O_3 clusters, and the coalescence of Al_2O_3 clusters to form a continuous film. In this context, Kim *et al* and Seo *et al* combined the ALI process with O_2 plasma pre-treatment to improve the barrier properties of flexible films, giving a WVTR value of $\sim 1.28 \times 10^{-5}$ g m^{-2} d^{-1} [69, 70]. In this system, pre-treatment with O_2 plasma can introduce additional oxygen groups to the surface to improve the adhesion of the Al_2O_3 film. Indeed, after 100 bending fatigue tests with a radius of 5 mm (figure 5(c)), the WVTR was slightly higher than it was without pre-treatment, demonstrating the excellent mechanical stability of the prepared polymer substrate [66]. In addition, Kim *et al* prepared hybrid films with a remarkable WVTR of 10^{-5} g m^{-2} $^{-1}$ and an impressive bending radius of 1.75 mm [36]. Similarly, Wang *et al* fabricated Alucone films via the PEMLD approach to give a WVTR of 10^{-5} g m^{-2} d^{-1} and a bending radius of 3 mm [71, 72].

In the context of flexible electronics, stretching devices require the highest encapsulation standards, as stretching deformation occurs in all layers rather than folding along a specific axis. PDMS, as a stretchable material, exhibits high transparency, flexibility, and stretchability, but presents poor barrier properties [73, 74]. Previously, our research group developed an inorganic–organic hybrid encapsulation structure by simply doping with silica nanoparticles and applying the ALI technique. Aging tests demonstrated that this strategy can achieve a high barrier performance, giving a low WVTR of 1.81×10^{-3} g m^{-2} d^{-1}. Even after thousands of cycles of 1% tensile strain, the film continued to maintain a low barrier rate (2.01×10^{-3} g m^{-2} d^{-1}). In addition, the encapsulated QD film exhibited excellent display properties when bending and stretching underwater, leading to a storage time of 2400 h and a PL intensity of >50% [75] (figure 5(d)). It is expected that ongoing research and innovation in the area of ALD will lead to the development of encapsulation structures with outstanding barrier properties that are capable of withstanding a small bending radius and a certain tensile strain. This achievement opens new possibilities for the application of OLED displays in more demanding environments. In addition, it will be necessary to assess the balance between the film's qualities and its flexibility in further detail.

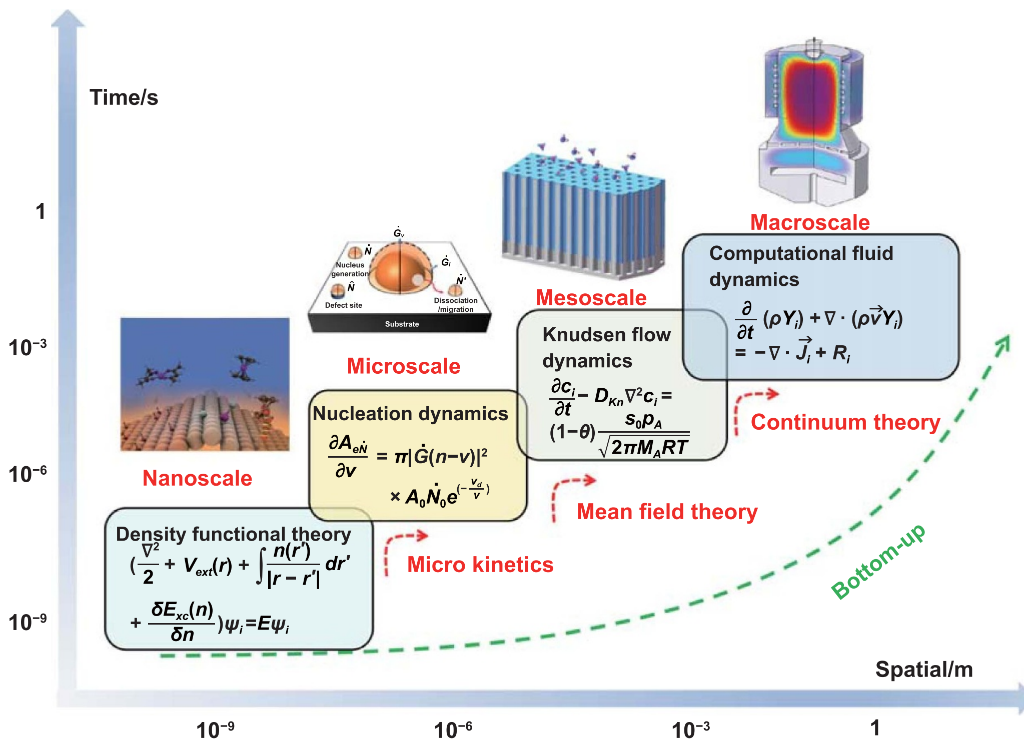

Figure 6. Schematic diagram of multi-scale simulations of the ALD, Reproduced with permission from [81]. Reprinted with permission from Lan Y X, Wen Y W, Li Y C, Yang J Q, Cao K, Shan B, Chen R 2023 'Selectivity dependence of atomic layer deposited MnOx on the precursor ligands on Pt facets', J. Vac. Sci. Technol. A 41 012402. Copyright 2023, American Vacuum Society. Reprinted from [82]. © 2023 Elsevier B.V. All rights reserved.

Hybrid organic–inorganic solutions appear promising; however, issues related to a mismatch between the thermal coefficient and the mechanical modulus lead to the requirement for specific fabrication conditions. The strain generated from such a mismatch can easily compromise devices or encapsulations, presenting another hurdle. Indeed, degradation of the hybrid layer during prolonged operation poses a substantial barrier to its commercialization.

2.4. Multi-scale simulations of the ALD manufacturing process

As mentioned above, ALD has been applied to the modification of QD-based devices across different scales; thus, multi-scale research and manufacturing methods are urgently required [77]. Thus, as presented in figure 6, first-principles calculations, nucleation dynamics [78], Knudsen flow dynamics, and computational fluid dynamics can be combined to achieve multi-scale simulations. The first-principles method provides the electronic and thermodynamic properties during the ALD reaction on the nanoscale. Using microkinetics, the calculated ALD reaction rate can be integrated into the nucleation model to provide important information regarding ALD nucleation at the microscale. To extend the mesoscale simulation, the mean field theory [79] provides a key link to couple the ALD nucleation kinetics and the Knudsen flow dynamics. Based on the continuum theory [80], the ALD diffusion and reaction in the features are coupled with the computation of fluid dynamics at the macroscale. With these considerations in mind, a cross-scale simulation method was established to clarify the ALD reaction mechanism, describe the ALD nucleation behavior, and optimize the ALD process.

To clarify the interactions between the ALD precursor and the QD surfaces, first-principles methods were used to investigate the adsorption energies, and the minimum energy paths of the precursors were calculated using the nudged elastic band method. It was found that TMA prefers to link the amine ligands and the QDs, rather than kick the ligands out. In another study, a benign and asymmetric aluminum precursor, namely methyl aluminum di-isopropoxide, was used to treat the QDs to avoid successive dissociation during the reaction with surface ligands, resulting in a nearly trap-state-free band structure of passivated QDs [83]. To evaluate the reactivity of the precursor on the substrate, a micro-kinetic method was developed to couple the adsorption energy and the reaction energy barrier with the aim of calculating the ALD reaction rate. Based on the microkinetics, the reactivity and selectivity of the Mn precursors were found to exhibit obvious dependence on the ligand structure [81]. This combination of first-principles calculations with the microkinetics method builds a bridge between the atomic site reaction rate and ALD nucleation, in addition to film growth when considering a larger-scale simulation.

At the microscale, targeted passivation of the pristine facets of QDs and selective filling of the pinholes in the functional layers are desired to prevent the recombination of nonradiative carriers in the PQLEDs. Thus, an anisotropic growth model was developed to describe the selective deposition and

nucleation delays [84] on different substrates (such as pristine and ligand-covered surfaces). This model provides a numerical representation of ALD growth and alignment, while fitting well with the experimental data. The interplay between nuclear expansion and diffusion in nongrowth regions is essential in this system. By incorporating parameters such as the initial defect density, the nucleus lateral expansion rate, the growth per cycle (GPC), and the nucleus diffusion probability, the robustness of the model was confirmed by its strong correlation with the experimental data. Furthermore, the model efficiently predicted the nucleation dynamics, such as the coverage and nucleation delay, under varying ALD conditions, including different purge times, temperatures, and pressures.

The reactor-scale model focuses on the multi-physical field coupling process of fluid dynamics, heat, and mass transfer, which is important for reactor design and the corresponding process optimization [85, 86]. Macroscopic parameters such as the partial pressure of the precursor at the reactor boundary were applied to the boundary conditions of the mesoscale model. In addition, the consumption of the precursor at the mesoscale was applied as a net flux through the substrate boundary and was coupled with mass transfer in the reactor-scale model. The high aspect ratio pores in size of micro meter lead to molecular flow state and the Knudsen diffusion applied in the mesoscale model [87]. The competitive effect of surface deposition with cross-scale precursor mass transfer was also analyzed to study the coating conformality in high-aspect-ratio structures. Moreover, different aspect ratios and specific surface areas correspond to different precursor consumptions, which can be accurately predicted by the model [82], enabling the design and optimization of ALD reactors. The influence of the ALD process parameters on the deposition rate and precursor usage was thoroughly investigated, and the optimum speed range was determined. It was found that coupled cross-scale simulations from the nano- to the macro-scales combined with the ALD reaction and the multi-physical field could provide important guidance for chamber design and process optimization. It is worth noting that many factors are still neglected at different scales owing to the model complexity. For example, the steric effect of the precursors and diffusion nuclei on the substrate may play an important role in ALD growth, which is yet to be considered in the context of mesoscale nucleation dynamics. It is therefore necessary to establish a universal and complete cross-scale model for ALD growth.

Approximately 80 000 articles related to ALD growth can be found currently in the Science Citation Index-Expanded, with the majority being independent reports. To facilitate the use of the reported ALD techniques in research, there is an urgent need to establish a comprehensive and standard database for ALD applications. An automatic framework was constructed to find and obtain ALD-relevant articles by the application programming interface request of publishers on the Internet. More recently, the artificial intelligence program ChatGPT has been used to extract key information regarding the film materials, precursors, growth temperatures, substrates, and the GPC. As a result, more than 2000 groups of ALD parameters have been obtained and integrated into an ALD technological database [88]. This database should provide a convenient search and screening of ALD technique parameters, aids the selection of ALD precursors and materials, and provides the underlying mechanisms responsible for the ALD film properties and performance.

3. Measurement methods for determining the quality of fabricated films

3.1. Highly precise detection of low-permeation coefficients

Permeation is a major problem that can lead to the degeneration [89] of luminescent materials that are sensitive to the environment (e.g. hydrogen-sensitive metallic structural materials, water vapor-sensitive OLED electroluminescent layers) [54, 90–92]. For example, trace gas permeation in the service environment leads to device failure and can even cause device explosion and radiation release. Thus, to evaluate trace gas permeation, suitable characterization methods and systems must be developed to measure the trace amounts of permeated gases. For example, mass spectrometry (MS), which exhibits high sensitivity and allows broad-spectrum detection, has been widely used for gas detection, such as in the analysis of multicomponent gases, the measurement of water, oxygen, and hydrogen isotopes, and the detection of other small molecules for highly sensitive permeation measurements.

Nörenberg *et al* [93] were the first to combine MS with permeation detection, proposing different measurement requirements for the analyses of inert gases (nitrogen, helium, and neon), small molecular weight gases (hydrogen), adsorbed gases (water), and organic gases. By detecting the permeation gas pressure, it was found that the lower limit of measurement for the permeation rates of inert gases by MS was $<1 \times e^{-3}$ g m^{-2} d^{-1}. Compared with traditional permeation detection methods, MS greatly improves the detection sensitivity. In this context, Nakano *et al* [94] combined MS-based gas partial pressure detection with numerical water permeability measurements to propose a barrier assessment tool for water vapor, and to introduce a cold trap enrichment method for condensed gas to amplify the weak permeation signal. As a result, the lower detection limit was increased to $1 \times e^{-5}$ g m^{-2} d^{-1}, and the sensitivity index for water permeation measurement was superior to the $5 \times e^{-5}$ g m^{-2} d^{-1} index reported for existing commercial devices, such as those represented by the MOCON® permeation detection instruments.

To evaluate the barrier performances of flexible organic packages, Kiese *et al* [96] developed an ultralow permeation measurement device based on a constant-flow carrier-gas system. This device was combined with MS to measure the transient and steady-state permeation activities of water vapor through a high-barrier membrane. The accumulation of permeated water vapor prior to transport to the detector allows for extremely low order of magnitude WVTR measurements, and the WVTR values measured using this device were found to be consistent with those determined using the commercially available MOCON® carrier gas device. However, it should be noted here that owing to differences in the structure and

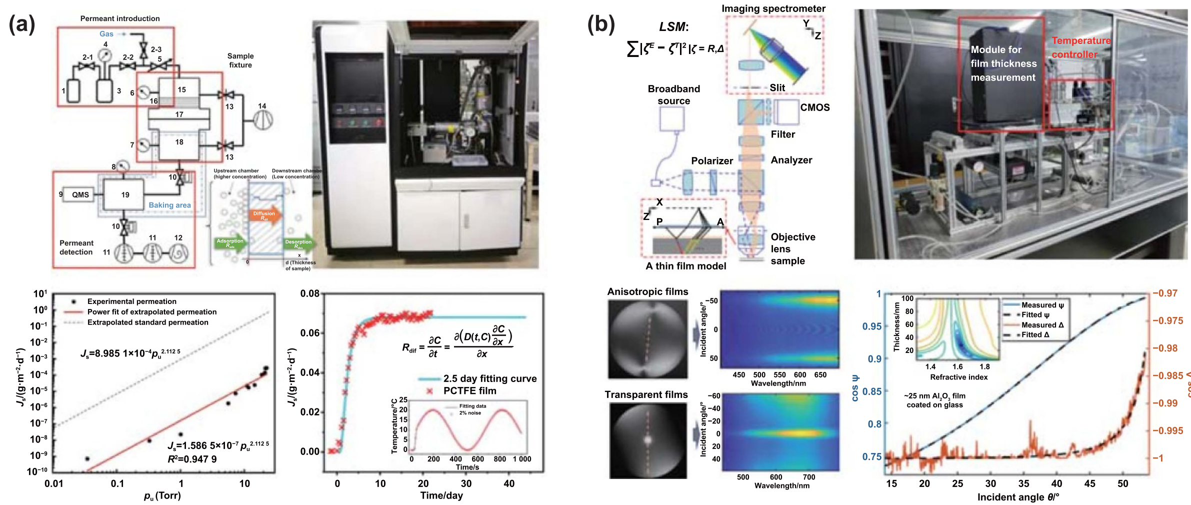

Figure 7. Schematic diagram of measurement. (a) The principle and equipment diagram of the permeation measurement system (top row), as well as the system calibration curve and PCTFE film test and prediction curve (bottom row). Reproduced from [95]. © 2021 THE AUTHORS. Published by Elsevier LTD on behalf of Chinese Academy of Engineering and Higher Education Press Limited Company. (b) A home-made PARS equipment with its schematic diagram (top row), the two work modes and a transparent film measurement sample (bottom row). Reproduced from [95]. © 2021 THE AUTHORS. Published by Elsevier LTD on behalf of Chinese Academy of Engineering and Higher Education Press Limited Company.

mass of the barrier film, the WVTR requires a certain amount of time to reach a steady-state value. As a result, the use of a non-steady-state measurement scheme in combination with the finite element method resulted in a more accurate estimation of the steady-state WVTR with a reduced measurement time.

In another study, permeation measurements with time-integrated enriched amplified signals have been carried out, and the lower limit of the barrier membrane permeability was determined to be the order of $1 \times e^{-5}$ g m^{-2} d^{-1} [95]. Figure 7(a) shows the principle of this system along with a photographic image of the setup. The calibration curve of the test system is also shown, along with an actual measurement and a fitted prediction curve for the poly(trifluorochloroethylene) (PCTFE) film. The schematic diagram of the test system shows the three main components, namely the inlet, the sample clamping, and the detector device. The basic steps and principles associated with film permeation are also shown. This system focused on measuring the entire film permeation process and obtaining the steady-state value of the permeation measurement. To minimize errors associated with the system itself and the nonlinearity of the equipment, a standard PEN film was used to calibrate the system, as shown in the figure. In addition, the actual measurement data for the PCTFE film and the permeation prediction curve for a period of 2.5 d (right-hand inset, figure 7(a)) are shown. It should be noted here that the permeation prediction can indicate the testing lifetime of high-barrier films [97], and machine learning methods can be used to predict the permeation behaviors of such films. However, current research is still struggling to break the lower limit of actual measurement ($1 \times e^{-6}$ g m^{-2} d^{-1}) to meet measurement demands. This is due to difficulties in reducing the signal-to-noise ratios of such measurements, along with improving the signal accumulation method, facilitating maintenance and processing of the vacuum system, and eliminating signal interference. Breakthroughs must therefore be made in the contexts of vacuum back-bottom signal enhancement, vacuum design, and maintenance.

3.2. Online and real-time monitoring of high-precision film growth

With the ongoing development of flexible electronics and displays, the application of organic films (e.g. PET and polyimide (PI) films) is rapidly increasing owing to their distinct physical properties, including bendability and roll-to-roll processing ability [98]. However, the anisotropic and transparent natures of such films pose a challenge in the context of online monitoring for conventional methods [99]. For example, the anisotropy leads to complications in terms of the parameters to be solved (e.g. the thickness and anisotropic refractive indices), and the transparent substrates tend to suffer from backside reflections. The former causes cross-polarization between the p- and s-orientations, while the latter causes depolarization owing to the incoherently reflected light from the backside of the substrate. In addition, although transmission-type methods [100–104], such as transmission ellipsometry and polariscopy, are sensitive to the anisotropy of the material, the signal from the coated thin film is comparatively less sensitive. Therefore, these methods are typically used for bulk anisotropic materials. In comparison, reflection methods are sensitive to interfaces and thin films, while being less sensitive to the substrate anisotropy. Therefore, reflection-type methods are more suitable for characterizing thin films presented on transparent anisotropic substrates.

The commonly used ellipsometry technique [102] can reduce backside reflection by polishing the rear surface of the

substrate or coating the backside with black paint; however, it cannot meet the cross-polarization requirements. In contrast, the more recently developed Mueller matrix ellipsometry can meet the anisotropy and depolarization issues [99]. In terms of the optical modeling problem, Postava *et al* [103] built an optical model of the mixing of coherent and incoherent light in anisotropic multilayer structures, and named this the coherent matrix model. Later, Nichols *et al* [104, 105] used their Mueller matrix polarimeter to test this incoherent light superposition model using several anisotropic slabs and metallic coatings on anisotropic crystals. However, they found that azimuthal angle scanning and assisted transmission ellipsometry were required to recover all parameters. Thus, to reduce the requirement for auxiliary measurements, conoscopy was introduced into the Mueller matrix-based method. More specifically, Arteaga and Kahr [106] observed several thin freestanding crystal slabs using a homemade Mueller matrix conoscope. Moreover, back focal plane (BFP)-related methods [107–109], such as angle-resolved ellipsometry and reflectometry, have been verified for their ability to carry out nanometer thin-film single-shot measurements. Such techniques have the potential to carry out rapid measurements on thin films that have been coated on anisotropic substrates. Indeed, this has been achieved upon combination with angle-resolved reflectometry and conoscopy using an incoherent light superposition optical model.

Figure 7(b) illustrates the polarized angle-resolved reflectometry (PARS) setup [109], which includes the illumination source, the measurement probe, and the detection unit. In this system, the collimated white light becomes linearly polarized after passing through a linear polarizer set at 0°, and is refocused on the BFP of the objective lens. The polarized light varies with the azimuthal incidence angle on the measured sample at various angles of incidence through the objective lens. The light is then reflected at the same angles, recollected by the objective lens, and focused on the BFP. After modulation by the analyzer (another linear polarizer set at 45°), the full azimuth and incident angle resolved spectra (FARS) are captured separately from the abstract wavelength and angle resolved scattering spectra using a complementary metal oxide semiconductor and an imaging spectrometer. Using a reference sample (e.g. a standard SiO_2 sample), the angle-resolved reflectance is then measured. The transparent film model shows that the reflective beam contains two incoherent parts, namely the reflectance from the upper coatings and the backside reflectance from the rear surface of the substrate. When the tested substrate is anisotropic, interference between the ordinary and extraordinary light from the backside reflection occurs.

To measure transparent films, two methods exist for dealing with backside reflections in the PARS system. One accounts for this in the analysis model, while the other is based on the use of spatial separation. More specifically, when a spatial separation is observed in the FARS image, the reflectance can filter out the backside reflection due to the large angle of light that is reflected from the backside out of the aperture. Therefore, a semi-infinite substrate model can be used to calculate the coating parameters. Upon extraction of the ellipsometry parameters ($\Psi(\theta)$, $\Delta(\theta)$) from the wanted reflectance, the fitting results for the thickness and the refractive index were found to be consistent with the commercial ellipsometer. The anisotropic film shown in the bottom left-hand panel of figure 7(b) shows an example accounting for such backside reflection. The FARS image provides the Euler rotation angle between the refractive index ellipsoidal coordinates and the x–y–z coordinate system, the anisotropic interference phase Δ_{oe}, and the reflectance R. With prior knowledge of the Euler angle, the thickness and refractive index can be determined by simultaneously fitting the Δ_{oe} phase and the reflectance to the theoretical coherency matrix model.

It has also been reported that the incoherent optics model and the PARS system can solve the demands for high-precision characterization of the optical anisotropy and thicknesses of transparent flexible films. However, with the advancement of large-scale and atomic-level manufacturing technologies, such as roll-to-roll ALD, new inspection requirements encompassing higher precisions, enhanced robustness parameters, increased efficiencies, and expanded measurement parameters are continuously being reported. These evolving demands pose significant challenges for the development of monitoring technologies.

The features associated with rapid and large-scale manufacturing not only impose elevated demands on the efficiencies of monitoring systems, but also significantly impact the reliability of the monitoring results owing to varying factors, including mechanical vibrations and temperature fluctuations. Although antivibration snapshot measurements have been developed, there is still a lack of robustness overall. Thus, the development of inline monitoring technologies with enhanced resistances to environmental perturbations is imperative. Additionally, flexible films are highly susceptible to mechanical stresses during processing, such as the tensile force experienced during the roll-to-roll process. These stresses can lead to the formation of folds, microcracks, and other morphological changes on the film surfaces. Consequently, it is necessary to accurately characterize the complete surface morphology of the film to provide feedback for manufacturing. However, current monitoring techniques, such as ellipsometry, are based on single-point measurements, and so are insufficient to meet the demands of such complex measurements. Moreover, achieving a nanometer-to-atomic-level accuracy poses additional challenges, particularly for thin films with complex surface morphologies or multiple layers. A synergistic combination of the advantageous features of multiple measurement techniques, such as the sub-nanometer precision of ellipsometry and the morphology measurement capabilities of spectral interferometry, could therefore be considered a promising method for achieving the high-precision inline monitoring of thin films with complex surface morphologies. Contemporary thin-film optical measurement technologies are not confined to the assessment of film thicknesses and optical refractive indices; rather, they are progressively expanding to encompass more physical and geometric parameters.

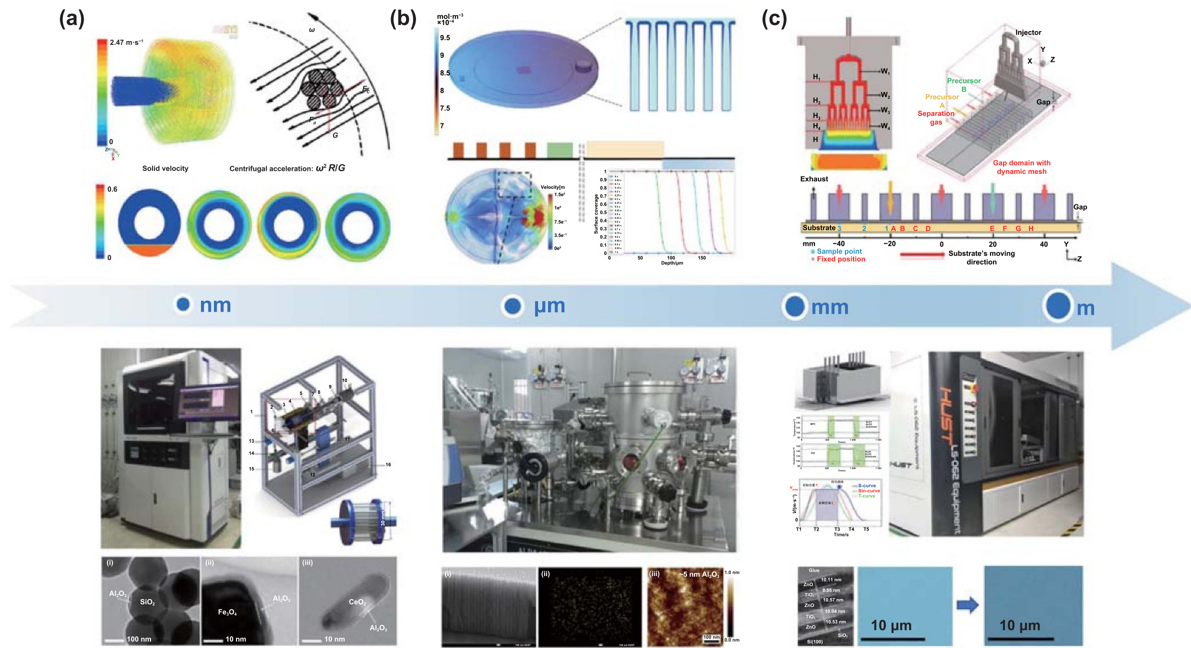

Figure 8. Equipment design and setup for ALD on (a) nanoparticles, Reprinted from [114], with the permission of AIP Publishing. (b) High-aspect-ratio structures, Reprinted from [116], with the permission of AIP Publishing. And (c) high-speed and large-area substrates, Reprinted from [86]. © 2020 Elsevier Ltd. All rights reserved. Reprinted from [120], with the permission of AIP Publishing.

4. ALD equipment for multi-scale manufacturing

4.1. Rotary ALD reactor for particle fluidization

In the context of phosphors, QDs, and other luminescence materials, it is necessary to achieve control of the atomic thickness, uniform surface modification, and the functionalization of nanoparticles with high specific surface areas. However, the nanoparticle agglomeration caused by strong cohesive forces is unfavorable for film conformality [110, 111] (figure 8(a)). Thus, a number of multi-scale ALD manufacturing methods have been developed to optimize the powder coverage, produce high-aspect-ratio structure coatings, and allow high-speed and large-area deposition.

For example, a fluidized bed coupled rotary ALD reactor was developed for the thin-film coating of nanoparticles via ALD. This reactor consists of a main reaction chamber, a pumping section, a dosing and fluidizing system, rotary manipulator components, and a double-layer cartridge for particle storage. In contrast to a traditional fluidized bed, the effective gravity of the particles is an independently controllable parameter in a centrifugal fluidized bed [112]. Upon increasing the rotation speed, the effective particle gravity increases to overcome the viscous shear force, which can cause particles to fall off from the aggregates. A centrifugal fluidized bed is therefore conducive to overcoming the problems of slugging, channeling, and particle clustering that are observed in traditional fluidized beds [113]. As a result, the transition from agglomerated fluidization to dispersed fluidization is promoted to improve the fluidization quality of the particles. Figure 8(a) shows another example of a rotary ALD reactor combined with fluidization to achieve the atomic layer coating of nanoparticles [114]. In this case, the cylindrical particle cartridge provides a fluidization function to disperse the particles, and high-speed rotation is employed to enhance the gas–solid interactions and ensure the uniform and continuous fluidization of the particle bed. The enlarged particle bed interstitials and enhanced gas–solid interactions facilitate precursor transport throughout the particle bed and reduce the processing time. In addition, the cartridge ensured that the flow of the precursors was confined only through the granulate bed to achieve high precursor utilization without static exposure, as confirmed by *in situ* MS measurements of both half-reactions. By optimizing the gas velocities and rotation speeds, the minimum pulse and purge times for a complete and uniform coating were shortened, and *in situ* MS showed that the precursor usage reached 90%. During the particle coating experiment, inductively coupled plasma–optical emission spectroscopy measurements suggested a saturated growth of nanoscale Al_2O_3 films on spherical SiO_2 nanoparticles. The uniformity and composition of the shells were examined using high-angle annular dark-field TEM and energy-dispersive x-ray spectroscopy. The morphology results of the Al_2O_3 coatings on the CeO_2 and SiO_2 nanoparticles confirmed the controllability and uniformity of coatings and their wide applicability on various nanostructures [114]. This rotary reactor affords a practical approach for particle ALD to achieve faster and more economical processes.

4.2. Conformal deposition for the production of high-aspect-ratio nanostructures

High-aspect-ratio nanostructures exist in spun and stacked luminescent materials, making ALD coating difficult. Upon

increasing the high-aspect-ratio integration density, a larger specific surface area is formed, which renders it more difficult to achieve a uniform and conformal deposition of thin films [115]. To investigate the controllable preparation of such a conformal thin film, an ALD instrument equipped with an *in situ* characterization ability was developed by integration with a quartz crystal microbalance, an ellipsometer, a quadrupole mass spectrometer, and an *in situ* infrared spectrometer (figure 8(b)) [114, 116]. This system permitted the precursor pulse process to be monitored, along with the stable precursor output and real-time monitoring of the species' partial pressure. Further explorations were also possible to investigate the effects of different process conditions, such as the temperature, gas flow rate, and pressure, on the thin film growth rate. It was found that the simulation results obtained using the multi-scale model agreed well with the experimental data recorded for nanopores with various aspect ratios. These observations confirm that such setups can provide guidance for process optimization to ultimately generate the uniform and conformal deposition of films. As a result, an ultrathin Co_3O_4 film was uniformly coated onto high-aspect-ratio (>100:1) TiO_2 nanotubes to improve the visible-light photoelectrochemical performance by an order of magnitude [117].

Furthermore, an integrated *in situ* thickness monitoring system was developed to monitor the deposition rate at the mouth of a high-aspect-ratio structure in real time. It is important to avoid unwanted CVD-type growth at the mouth of the hole to ensure conformal coating. It was found that changing the position of the gas flow and the substrate from parallel to vertical effectively improved both the uniformity and the conformality. This is crucial for enhancing the precursor flux into high-aspect-ratio structures and compensating for the adverse effects of diffusion restrictions. Moreover, a high-vacuum system was also introduced, which allowed precise control of the reactor pressure over the high-vacuum range and through high pumping speeds, thereby accelerating the purging of excess precursors and by-products that remain in the high-aspect-ratio structure. As a result, the purging time is reduced, and the film quality is improved.

4.3. Spatial ALD for rapid and large-area manufacturing

Among the various ALD techniques reported to date, the spatial ALD method effectively meets the high throughput and low cost requirements of many applications [118]. In comparison with conventional time-sequencing ALD processes, the two half-reactions in spatial ALD are separated in different reaction areas using inert gases as physical barriers. This eliminates the need for time-consuming purge steps. As a result, the deposition rate can be increased by 1–2 orders of magnitude by increasing the relative gas flow velocity between the injector and the substrate [119].

An SALD reactor integrated with modular injectors was later designed to increase deposition efficiency and maintain a high film smoothness and uniformity. As shown in figure 8(c), a modular injector possessing multilayer structured channels was designed to improve the homogeneity of gas distribution in the reaction zone [120]. For atmospheric SALD systems, a modular injector was designed to improve the efficiency and expandability of the deposition system. The modular injector consisted of a single precursor channel, an oxidant co-reactant channel, three separation channels, and four outlets for the byproducts and excess gases. The isolator channel was surrounded on both sides to ensure good isolation from any water and oxygen presented in the atmosphere. The reaction area width was set to 250 mm. Considering the thermal deformation and cross-contamination of the precursors, the thicknesses of the nozzle and the exhaust channel were designed to be 14 mm and 1 mm, respectively. The injectors were modular in nature, and allowed both vertical and parallel substrate movement, thereby enabling larger deposition areas and an increased wafer throughput. To withstand the elevated temperatures and the corrosive nature of the precursors, the injector was constructed from a lightweight aluminum alloy that possesses excellent corrosion resistance and high thermal conductivity. The non-uniformity of the film deposition rate distribution was maintained within 3% under different substrate moving speeds, and upon comparison with the ordinary rectangular channels, the deposition uniformity was significantly improved. These observations clearly demonstrate the advantages of the multilayer gas separation structure in the uniform growth of thin films.

It was also reported that the number of modular injectors could be expanded to form nozzle groups for larger deposition areas and faster deposition rates, thereby extending the manufacturing scale. To improve the dynamic performance of the SALD system, an S-motion curve algorithm based on an asymmetric polynomial was adopted to overcome the problems associated with sudden changes in velocity and the high levels of acceleration in the traditional T-shaped motion curve algorithm [120]. This algorithm effectively reduced the inertial shock and residual vibrations of the system caused by the base motion, and reduced the displacement error of the base by >80%. Based on an efficient modular spatial ALD system assisted by multi-scale modeling optimization, the maximum deposition rate reached 100 nm min^{-1}, leading to an efficient, fast, and uniform preparation of nanoscale thin films. It should be noted here that the deposition rate in SALD is primarily influenced by the precursor concentration, the exposure time, and the deposition temperature. It was found that the precursor exhibited the highest adsorption rate within the optimal temperature window for SALD deposition. Although it was possible to reduce the exposure time by increasing the precursor concentration to give an improved deposition rate, this poses challenges owing to the drag effect of the fluid during substrate motion [86]. This, in turn, can result in a reduced precursor concentration within the deposition area and potential cross-contamination between the different precursors, thereby exacerbating chamber pollution [121, 122]. The future development of flexible display production techniques will also require the incorporation of a roll-to-roll operation, which causes vibration, deviation, and tension control issues, ultimately necessitating the implementation of additional hardware.

Overall, the above studies indicate that rotary ALD is beneficial for the deposition of particles such as QDs and nanoparticles. For high-aspect-ratio or complex structures, planar ALD with a long exposure ensures conformal deposition, while SALD offers the possibility of large-area high-speed deposition. A combination of ALD tools is, therefore, often necessary to achieve the desired deposition characteristics on different scales. For display development, the growth rate, film quality, uniformity, and efficiency are the key elements that require optimization in the future.

5. Conclusion and perspective

To address the stability and efficiency challenges encountered in the manufacturing of luminescent materials for displays, ALD has been incorporated across different scales of manufacturing. At the atomic scale, ALD is employed for the precise passivation and surface coating of nanocrystals and phosphors, thereby enhancing the stability of luminescent materials. At the device scale, ALD is used to fabricate dual-HILs and ETLs and to fill in the emissive layers, while also modifying the interfaces between these functional layers. This results in a material with well-balanced carrier transport properties, high moisture resistance, and an excellent luminescence lifetime. On the display scale, composite barrier functional layers have been designed and fabricated by optimizing the deposition process parameters and the encapsulation layer, enhancing both the flexibility and stability of the resulting material. In addition, three types of ALD reactors were developed to achieve the conformal deposition of nanoparticles, high-aspect-ratio nanostructures, and large-area substrates. Furthermore, advanced measurement and online real-time monitoring systems have been used to assess properties such as barrier resistance, film thickness, and roughness. Moreover, cross-scale simulations were conducted to delineate the microscopic surface reaction mechanism, the mesoscopic nucleation dynamics, and the macroscopic deposition processes across the temporal and spatial scales. The obtained results serve to optimize the ALD process throughout the cross-scale manufacturing of flexible display devices. Overall, ALD shows immense potential for achieving precise control of surface passivation, device fabrication, and flexible encapsulation processes. It also meets the requirements of cross-scale fabrication and can be integrated into the current streamline of large-scale production owing to its compatibility with manufacturing processes.

Acknowledgments

This work is supported by the National Natural Science Foundation of China (51835005, 52273237), the National Key R&D Program of China (2022YFF1500400), and the New Cornerstone Science Foundation through the XPLORER PRIZE. The authors would like to acknowledge the assistance from Di Wen, Min Wang, Zoushuang Li, Lihua Peng for preparing the article. The authors also acknowledge the support from the Flexible Electronics Research Center, the Analytic Testing Center, and the Optoelectronic Micro&Nano Fabrication and Characterizing Facility at the WNLO of HUST.

ORCID iD

Rong Chen https://orcid.org/0000-0001-7371-1338

References

[1] Kagan C R, Lifshitz E, Sargent E H and Talapin D V 2016 Building devices from colloidal quantum dots *Science* **353** aac5523
[2] Bera S and Pradhan N 2020 Perovskite nanocrystal heterostructures: synthesis, optical properties, and applications *ACS Energy Lett.* **5** 2858–72
[3] Chen L, Cheng Z M, Zheng G F, Yao G, He L R, Wang L, Liu J Z, Zheng H W, Wei S Z and Ni H Y 2021 A third route to synthesis of green phosphor $SrSi_2O_2N_2:Eu^{2+}$ from SrO *J. Lumin.* **230** 117729
[4] Macpherson S *et al* 2022 Local nanoscale phase impurities are degradation sites in halide perovskites *Nature* **607** 294–300
[5] Liu M M *et al* 2021 Suppression of temperature quenching in perovskite nanocrystals for efficient and thermally stable light-emitting diodes *Nat. Photon.* **15** 379–85
[6] Li Y, Li Q L, Li Y, Yang Y L, Zhang S L, Zhao J T, Wan J Q and Zhang Z J 2023 Water-assistant ultrahigh fluorescence enhancement in perovskite polymer-encapsulated film for flexible x-ray scintillators *Chem. Eng. J.* **452** 139132
[7] Liu Y C, Chen T, Jin Z K, Li M X, Zhang D D, Duan L, Zhao Z G and Wang C 2022 Tough, stable and self-healing luminescent perovskite-polymer matrix applicable to all harsh aquatic environments *Nat. Commun.* **13** 1338
[8] Xu W T, Zhou Y F, Huang D C, Su M Y, Wang K, Xiang M and Hong M C 2015 Luminescent sensing profiles based on anion-responsive lanthanide(III) quinolinecarboxylate materials: solid-state structures, photophysical properties, and anionic species recognition *J. Mater. Chem.* C **3** 2003–15
[9] Tsai Y T, Chiang C Y, Zhou W Z, Lee J F, Sheu H S and Liu R S 2015 Structural ordering and charge variation induced by cation substitution in (Sr, Ca)$AlSiN_3$:Eu phosphor *J. Am. Chem. Soc.* **137** 8936–9
[10] Li Z B, Seto T and Wang Y H 2020 Enhanced crystallinity and thermal stability of Ba^{2+} and Al^{3+}-O^{2-} co-substituted $Sr_2Si_5N_8:Eu^{2+}$ *J. Mater. Chem.* C **8** 9874–84
[11] Feldmann S, Gangishetty M K, Bravić I, Neumann T, Peng B, Winkler T, Friend R H, Monserrat B, Congreve D N and Deschler F 2021 Charge carrier localization in doped perovskite nanocrystals enhances radiative recombination *J. Am. Chem. Soc.* **143** 8647–53
[12] Bian H, Wang Q, Yang S W, Yan C J, Wang H R, Liang L, Jin Z W, Wang G and Liu S Z 2019 Nitrogen-doped graphene quantum dots for 80% photoluminescence quantum yield for inorganic γ-$CsPbI_3$ perovskite solar cells with efficiency beyond 16% *J. Mater. Chem.* A **7** 5740–7
[13] Xiang F M, Givens T M, Ward S M and Grunlan J C 2015 Elastomeric polymer multilayer thin film with sustainable gas barrier at high strain *ACS Appl. Mater. Interfaces* **7** 16148–51
[14] Liu Y W, Tang A, Tan J H, Li Y H, Wu D, Zhang X, Zhao X Q, He P and Zhang H L 2020 High-barrier polyimide containing fluorenol moiety: gas barrier

properties and molecular simulations *React. Funct. Polym.* **157** 104747
[15] Zhu L J, Babu S S, Yu Q X, Long Y B, Zheng Z B, Wu H Y, Liu S W, Chi Z G, Zhang Y and Xu J R 2020 Transparent flexible ultra-low permeability encapsulation film: fusible glass fired on heat-resistant polyimide membrane *Adv. Mater. Interfaces* **7** 2001170
[16] Palmstrom A F, Santra P K and Bent S F 2015 Atomic layer deposition in nanostructured photovoltaics: tuning optical, electronic and surface properties *Nanoscale* **7** 12266–83
[17] George S M 2010 Atomic layer deposition: an overview *Chem. Rev.* **110** 111–31
[18] Bakke J R, Pickrahn K L, Brennan T P and Bent S F 2011 Nanoengineering and interfacial engineering of photovoltaics by atomic layer deposition *Nanoscale* **3** 3482–508
[19] Zhao Y J, Yin L J, ten Kate O M, Dierre B, Abellon R, Xie R J, van Ommen J R and Hintzen H T 2019 Enhanced thermal degradation stability of the $Sr_2Si_5N_8$:Eu^{2+} phosphor by ultra-thin Al_2O_3 coating through the atomic layer deposition technique in a fluidized bed reactor *J. Mater. Chem.* C **7** 5772–81
[20] Sanders B W 1993 Atomic layer epitaxy of phosphor thin films *Solid State Luminescence: Theory, Materials and Devices* ed A H Kitai (Springer) pp 293–312
[21] Li Y *et al* 2023 Self-aligned patterning of tantalum oxide on Cu/SiO_2 through redox-coupled inherently selective atomic layer deposition *Nat. Commun.* **14** 4493
[22] Kumah D P, Ngai J H and Kornblum L 2020 Epitaxial oxides on semiconductors: from fundamentals to new devices *Adv. Funct. Mater.* **30** 1901597
[23] Wei H Y, Wu J H, Qiu P, Liu S J, He Y F, Peng M Z, Li D M, Meng Q B, Zaera F and Zheng X H 2019 Plasma-enhanced atomic-layer-deposited gallium nitride as an electron transport layer for planar perovskite solar cells *J. Mater. Chem.* A **7** 25347–54
[24] Abelson A, Qian C, Salk T, Luan Z Y, Fu K, Zheng J G, Wardini J L and Law M 2020 Collective topo-epitaxy in the self-assembly of a 3D quantum dot superlattice *Nat. Mater.* **19** 49–55
[25] Woo J H, Koo D, Kim N H, Kim H, Song M H, Park H and Kim J Y 2021 Amorphous alumina film robust under cyclic deformation: a highly impermeable and a highly flexible encapsulation material *ACS Appl. Mater. Interfaces* **13** 46894–901
[26] Geng S C, Wen Y W, Zhou B Z, Wang Z J, Wang Z J, Wang P F, Jing Y, Cao K, Wang K and Chen R 2021 High luminance and stability of perovskite quantum dot light-emitting diodes via $ZnBr_2$ passivation and an ultrathin Al_2O_3 barrier with improved carrier balance and ion diffusive inhibition *ACS Appl. Electron. Mater.* **3** 2362–71
[27] Jing Y, Cao K, Zhou B Z, Geng S C, Wen Y W, Shan B and Chen R 2020 Two-step hybrid passivation strategy for ultrastable photoluminescence perovskite nanocrystals *Chem. Mater.* **32** 10653–62
[28] Fang F *et al* 2020 Atomic layer deposition assisted encapsulation of quantum dot luminescent microspheres toward display applications *Adv. Opt. Mater.* **8** 1902118
[29] Wang P F, Qin L, Zhou B Z, Liu M J, Geng S C, Wang M, Lei Z Y, Wen Y W and Chen R 2022 Boosted efficiency and lifetime of perovskite quantum dots light-emitting diode via NiO_x/PEDOT:PSS dual hole injection layers *Appl. Phys. Lett.* **120** 033502
[30] Zhou B Z, Wang P F, Geng S C, Wang M, Qin L, Wen Y W and Chen R 2021 Highly efficient $CsPbBr_3$ perovskite nanocrystal light-emitting diodes with enhanced stability via colloidal layer-by-layer deposition *ACS Appl. Electron. Mater.* **3** 2398–406
[31] Loiudice A, Saris S, Oveisi E, Alexander D T L and Buonsanti R 2017 $CsPbBr_3$ QD/AlO_x inorganic nanocomposites with exceptional stability in water, light, and heat *Angew. Chem., Int. Ed.* **56** 10696–701
[32] Xiang Q Y, Zhou B Z, Cao K, Wen Y W, Li Y, Wang Z J, Jiang C C, Shan B and Chen R 2018 Bottom up stabilization of $CsPbBr_3$ quantum dots-silica sphere with selective surface passivation via atomic layer deposition *Chem. Mater.* **30** 8486–94
[33] Likovich E M, Jaramillo R, Russell K J, Ramanathan S and Narayanamurti V 2011 High-current-density monolayer CdSe/ZnS quantum dot light-emitting devices with oxide electrodes *Adv. Mater.* **23** 4521–5
[34] Zhou B Z, Qin L, Wang P F, Chen Z, Zang J F, Zhang J B, Wen Y W and Chen R 2023 Fabrication of ZnO dual electron transport layer via atomic layer deposition for highly stable and efficient $CsPbBr_3$ perovskite nanocrystals light-emitting diodes *Nanotechnology* **34** 025203
[35] Yang Y Q, Duan Y, Chen P, Sun F B, Duan Y H, Wang X and Yang D 2013 Realization of thin film encapsulation by atomic layer deposition of Al_2O_3 at low temperature *J. Phys. Chem.* C **117** 20308–12
[36] Kim S H, Song S Y, Kim S Y, Chang M W, Kwon H J, Yoon K H, Sung W Y, Sung M M and Chu H Y 2022 A compact polymer–inorganic hybrid gas barrier nanolayer for flexible organic light-emitting diode displays *npj Flex Electron.* **6** 21
[37] Dey A *et al* 2021 State of the art and prospects for halide perovskite nanocrystals *ACS Nano* **15** 10775–981
[38] Ho K, Wei M Y, Sargent E H and Walker G C 2021 Grain transformation and degradation mechanism of formamidinium and cesium lead iodide perovskite under humidity and light *ACS Energy Lett.* **6** 934–40
[39] Chen Z, Zhou B Z, Yuan J H, Tang N, Lian L Y, Qin L, Zhu L H, Zhang J B, Chen R and Zang J F 2021 Cu^{2+}-doped $CsPbI_3$ nanocrystals with enhanced stability for light-emitting diodes *J. Phys. Chem. Lett.* **12** 3038–45
[40] Chen R, Liu M J, Wang M, Zhang Y H, Shan B and Cao K 2022 Acid-mediated phase transition synthesis of stable nanocrystals for high-power LED backlights *Nanoscale* **14** 13628–38
[41] Jing Y, Merkx M J M, Cai J M, Cao K, Kessels W M M, Mackus A J M and Chen R 2020 Nanoscale encapsulation of perovskite nanocrystal luminescent films via plasma-enhanced SiO_2 atomic layer deposition *ACS Appl. Mater. Interfaces* **12** 53519–27
[42] Zhao M, Cao K, Liu M J, Zhang J, Chen R, Zhang Q Y and Xia Z G 2020 Dual-shelled $RbLi(Li_3SiO_4)_2$:Eu^{2+}@Al_2O_3@ODTMS phosphor as a stable green emitter for high-power LED backlights *Angew. Chem., Int. Ed.* **59** 12938–43
[43] Liu Y B, Feng F, Zhang K, Jiang F L, Chan K W, Kwok H S and Liu Z J 2022 Analysis of size dependence and the behavior under ultrahigh current density injection condition of GaN-based Micro-LEDs with pixel size down to 3 μm *J. Appl. Phys.* **55** 315107
[44] Kramer I J and Sargent E H 2011 Colloidal quantum dot photovoltaics: a path forward *ACS Nano* **5** 8506–14
[45] Li G R *et al* 2016 Highly efficient perovskite nanocrystal light-emitting diodes enabled by a universal crosslinking method *Adv. Mater.* **28** 3528–34
[46] Asundi A S, Raiford J A and Bent S F 2019 Opportunities for atomic layer deposition in emerging energy technologies *ACS Energy Lett.* **4** 908–25
[47] Zhou B Z, Wang Z J, Geng S C, Li Y, Wang K, Cao K, Wen Y W and Chen R 2020 Interface engineering of

$CsPbBr_3$ nanocrystal light-emitting diodes via atomic layer deposition *Phys. Status Solidi* **14** 2000083
[48] Zhou B Z, Liu M J, Wen Y W, Li Y and Chen R 2020 Atomic layer deposition for quantum dots based devices *Opto-Electron. Adv.* **3** 190043
[49] Thimsen E, Johnson M, Zhang X, Wagner A J, Mkhoyan K A, Kortshagen U R and Aydil E S 2014 High electron mobility in thin films formed via supersonic impact deposition of nanocrystals synthesized in nonthermal plasmas *Nat. Commun.* **5** 5822
[50] Ji W Y, Shen H B, Zhang H, Kang Z H and Zhang H Z 2018 Over 800% efficiency enhancement of all-inorganic quantum-dot light emitting diodes with an ultrathin alumina passivating layer *Nanoscale* **10** 11103–9
[51] Yoon S H *et al* 2019 Insertion of an inorganic barrier layer as a method of improving the performance of quantum dot light-emitting diodes *ACS Photonics* **6** 743–8
[52] Lu Q, Yang Z C, Meng X, Yue Y F, Ahmad M A, Zhang W J, Zhang S S, Zhang Y Q, Liu Z H and Chen W 2021 A review on encapsulation technology from organic light emitting diodes to organic and perovskite solar cells *Adv. Funct. Mater.* **31** 2100151
[53] Kwon B H *et al* 2021 Organic/Inorganic hybrid thin-film encapsulation using inkjet printing and PEALD for industrial large-area process suitability and flexible OLED application *ACS Appl. Mater. Interfaces* **13** 55391–402
[54] Li Y, Cao K, Xiong Y F, Yang H Z, Zhang Y H, Lin Y, Zhou B Z, Huang J and Chen R 2020 Composite encapsulation films with ultrahigh barrier performance for improving the reliability of blue organic light-emitting diodes *Adv. Mater. Interfaces* **7** 2000237
[55] Behrendt A, Friedenberger C, Gahlmann T, Trost S, Becker T, Zilberberg K, Polywka A, Görrn P and Riedl T 2015 Highly robust transparent and conductive gas diffusion barriers based on tin oxide *Adv. Mater.* **27** 5961–7
[56] Chou C T, Yu P W, Tseng M H, Hsu C C, Shyue J J, Wang C C and Tsai F Y 2013 Transparent conductive gas-permeation barriers on plastics by atomic layer deposition *Adv. Mater.* **25** 1750–4
[57] Li Y, Xiong Y F, Cao W R, Zhu Q Q, Lin Y, Zhang Y H, Liu M J, Yang F, Cao K and Chen R 2021 Flexible PDMS/Al_2O_3 nanolaminates for the encapsulation of blue OLEDs *Adv. Mater. Interfaces* **8** 2100872
[58] Carcia P F, McLean R S, Reilly M H, Groner M D and George S M 2006 Ca test of Al_2O_3 gas diffusion barriers grown by atomic layer deposition on polymers *Appl. Phys. Lett.* **89** 031915
[59] Paetzold R, Winnacker A, Henseler D, Cesari V and Heuser K 2003 Permeation rate measurements by electrical analysis of calcium corrosion *Rev. Sci. Instrum.* **74** 5147–50
[60] Park S H K, Oh J, Hwang C S, Lee J I, Yang Y S and Chu H Y 2005 Ultrathin film encapsulation of an OLED by ALD *Electrochem. Solid-State Lett.* **8** H21
[61] Kim H G and Kim S S 2011 Aluminum oxide barrier coating on polyethersulfone substrate by atomic layer deposition for barrier property enhancement *Thin Solid Films* **520** 481–5
[62] Wang H R, Wang Z Y, Xu X C, Liu Y F, Chen C, Chen P, Hu W and Duan Y 2019 Multiple short pulse process for low-temperature atomic layer deposition and its transient steric hindrance *Appl. Phys. Lett.* **114** 201902
[63] Fahlteich J, Schönberger W, Fahland M and Schiller N 2011 Characterization of reactively sputtered permeation barrier materials on polymer substrates *Surf. Coat. Technol.* **205** S141–4
[64] Trung T Q, Kim C, Lee H B, Cho S M and Lee N E 2020 Toward a stretchable organic light-emitting diode on 3D microstructured elastomeric substrate and transparent hybrid anode *Adv. Mater. Technol.* **5** 1900995
[65] Wilson C A, Grubbs R K and George S M 2005 Nucleation and growth during Al_2O_3 atomic layer deposition on polymers *Chem. Mater.* **17** 5625–34
[66] Li Y, Wen D, Zhang Y H, Lin Y, Cao K, Yang F and Chen R 2021 Highly-stable PEN as a gas-barrier substrate for flexible displays *via* atomic layer infiltration *Dalton. Trans.* **50** 16166–75
[67] Chen T N, Wuu D S, Wu C C, Chiang C C, Chen Y P and Horng R H 2006 High-performance transparent barrier films of SiO_x/SiN_x stacks on flexible polymer substrates *J. Electrochem. Soc.* **153** F244
[68] Jeong E G, Kwon S, Han J H, Im H G, Bae B S and Choi K C 2017 A mechanically enhanced hybrid nano-stratified barrier with a defect suppression mechanism for highly reliable flexible OLEDs *Nanoscale* **9** 6370–9
[69] Kim L H, Kim K, Park S, Jeong Y J, Kim H, Chung D S, Kim S H and Park C E 2014 Al_2O_3/TiO_2 nanolaminate thin film encapsulation for organic thin film transistors via plasma-enhanced atomic layer deposition *ACS Appl. Mater. Interfaces* **6** 6731–8
[70] Seo S W, Jung E, Lim C, Chae H and Cho S M 2012 Water permeation through organic-inorganic multilayer thin films *Thin Solid Films* **520** 6690–4
[71] Wang Z Y, Wang J T, Li Z, Chen Z Q, Shangguan L C, Fan S Y and Duan Y 2023 Crosslinking and densification by Plasma-enhanced molecular layer deposition for hermetic seal of flexible perovskite solar cells *Nano Energy* **109** 108232
[72] Wang Z Y, Chen Z Q, Wang J T, Shangguan L C, Fan S Y and Duan Y 2023 Realization of an autonomously controllable process for atomic layer deposition and its encapsulation application in flexible organic light-emitting diodes *Opt. Express* **31** 21672–88
[73] Mahmood S, Khan A, Kant C, Chu C W, Katiyar M and Lin H C 2023 Transparent, stretchable, and self-healable gas barrier films with 2D nanoplatelets for flexible electronic device packaging applications *Adv. Mater. Interfaces* **10** 2202093
[74] Chen J W, Zhu Y T, Chang X H, Pan D, Song G, Guo Z H and Naik N 2021 Recent progress in essential functions of soft electronic skin *Adv. Funct. Mater.* **31** 2104686
[75] Zhang Y H, Wen D, Liu M J, Li Y, Lin Y, Cao K, Yang F and Chen R 2022 Stretchable PDMS encapsulation via SiO_2 doping and atomic layer infiltration for flexible displays *Adv. Mater. Interfaces* **9** 2101857
[76] Li Y, Xiong Y F, Yang Z H, Cao K and Chen R 2020 Thin film encapsulation for the organic light-emitting diodes display via atomic layer deposition *J. Mater. Res.* **35** 681–700
[77] Yun S, Wang H, Tom M, Ou F Y, Orkoulas G and Christofides P D 2023 Multiscale CFD modeling of area-selective atomic layer deposition: application to reactor design and operating condition calculation *Coatings* **13** 558
[78] Nguyen C T *et al* 2022 Gradient area-selective deposition for seamless gap-filling in 3D nanostructures through surface chemical reactivity control *Nat. Commun.* **13** 7597
[79] Fang W Z, Tang Y Q, Ban C M, Kang Q J, Qiao R and Tao W Q 2019 Atomic layer deposition in porous electrodes: a pore-scale modeling study *Chem. Eng. J.* **378** 122099
[80] Yim J, Verkama E, Velasco J A, Arts K and Puurunen R L 2022 Conformality of atomic layer deposition in microchannels: impact of process parameters on the simulated thickness profile *Phys. Chem. Chem. Phys.* **24** 8645–60

[81] Lan Y X, Wen Y W, Li Y C, Yang J Q, Cao K, Shan B and Chen R 2023 Selectivity dependence of atomic layer deposited manganese oxide on the precursor ligands on platinum facets *J Vac. Sci. Technol.* A **41** 012402
[82] Chen Y X, Li Z S, Dai Z A, Yang F, Wen Y W, Shan B and Chen R 2023 Multiscale CFD modelling for conformal atomic layer deposition in high aspect ratio nanostructures *Chem. Eng. J.* **472** 144944
[83] Wang Z J, Liu Z, Cao K, Wen Y W, Chen R and Shan B 2022 First-principles study of electronic properties of amine ligand-capped $CsPbBr_3$ surface with organo-metallic alumina precursor treatment *Appl. Surf. Sci.* **600** 154070
[84] Zheng Y X, Hong S, Psofogiannakis G, Rayner G B Jr, Datta S, Van Duin A C T and Engel-Herbert R 2017 Modeling and in situ probing of surface reactions in atomic layer deposition *ACS Appl. Mater. Interfaces* **9** 15848–56
[85] Shaeri M R, Jen T C, Yuan C Y and Behnia M 2015 Investigating atomic layer deposition characteristics in multi-outlet viscous flow reactors through reactor scale simulations *Int. J. Heat Mass Transfer* **89** 468–81
[86] Cong W T, Li Z S, Cao K, Feng G and Chen R 2020 Transient analysis and process optimization of the spatial atomic layer deposition using the dynamic mesh method *Chem. Eng. Sci.* **217** 115513
[87] Poodt P, Mameli A, Schulpen J, Kessels W M M and Roozeboom F 2017 Effect of reactor pressure on the conformal coating inside porous substrates by atomic layer deposition *J. Vac. Sci. Technol.* A **35** 021502
[88] Li H J , Wang Z J , Wen Y W , Shan B and Chen R 2022 Catalyst Hub (available at: www.catalysthub.net/ALDdatabase.php)
[89] Sun P Z *et al* 2020 Limits on gas impermeability of graphene *Nature* **579** 229–32
[90] Zhou K G *et al* 2018 Electrically controlled water permeation through graphene oxide membranes *Nature* **559** 236–40
[91] Franklin A D 2015 Nanomaterials in transistors: from high-performance to thin-film applications *Science* **349** aab2750
[92] Park J, Heo S, Park K, Song M H, Kim J Y, Kyung G, Ruoff R S, Park J U and Bien F 2017 Research on flexible display at Ulsan national institute of science and technology *npj Flex Electron.* **1** 9
[93] Nörenberg H, Miyamoto T, Tsukahara Y, Smith G D W and Briggs G A D 1999 Mass spectrometric estimation of gas permeation coefficients for thin polymer membranes *Rev. Sci. Instrum.* **70** 2414–20
[94] Nakano Y, Yanase T, Nagahama T, Yoshida H and Shimada T 2016 Accurate and stable equal-pressure measurements of water vapor transmission rate reaching the 10^{-6} g m^{-2} day^{-1} range *Sci. Rep.* **6** 35408
[95] Wanyan J, Cao K, Chen Z P, Li Y, Liu C X, Wu R Q, Zhang X D and Chen R 2021 A predictive instrument for sensitive and expedited measurement of ultra-barrier permeation *Engineering* **7** 1459–68
[96] Kiese S, Kücükpinar E, Reinelt M, Miesbauer O, Ewender J and Langowski H C 2017 A systematic approach for the accurate and rapid measurement of water vapor transmission through ultra-high barrier films *Rev. Sci. Instrum.* **88** 025108
[97] Chen Z P, Cao K, Wu R Q, Zhang L C, Zhang X D and Chen R 2022 Empirical model and PSO-based algorithm for efficient measurement of gas permeation through high barrier *IEEE Trans. Instrum. Meas.* **71** 7501308
[98] MacDonald W A, Looney M K, Mackerron D, Eveson R, Adam R, Hashimoto K and Rakos K 2007 Latest advances in substrates for flexible electronics *J. Soc. Inf. Disp.* **15** 1075–83
[99] Hong N N, Synowicki R A and Hilfiker J N 2017 Mueller matrix characterization of flexible plastic substrates *Appl. Surf. Sci.* **421** 518–28
[100] Arteaga O, Freudenthal J, Nichols S, Canillas A and Kahr B 2014 Transmission ellipsometry of anisotropic substrates and thin films at oblique incidence. Handling multiple reflections *Thin Solid Films* **571** 701–5
[101] Luders D D, Arcolezi G M, Pereira M L G, Braga W S, Santos O R, Simões M, Kimura N M, Sampaio A R and Palangana A J 2021 Conoscopic image of a biaxial negative in a reentrant discotic—biaxial nematic phase transition *Liq. Cryst.* **48** 974–9
[102] Aspnes D E 2014 Spectroscopic ellipsometry—Past, present, and future *Thin Solid Films* **571** 334–44
[103] Postava K, Yamaguchi T and Kantor R 2002 Matrix description of coherent and incoherent light reflection and transmission by anisotropic multilayer structures *Appl. Opt.* **41** 2521–31
[104] Nichols S, Arteaga O, Martin A and Kahr B 2015 Measurement of transmission and reflection from a thick anisotropic crystal modeled by a sum of incoherent partial waves *J. Opt. Soc. Am.* A **32** 2049–57
[105] Nichols S M, Arteaga O, Martin A T and Kahr B 2017 Partially coherent light propagation in stratified media containing an optically thick anisotropic layer *Appl. Surf. Sci.* **421** 571–7
[106] Arteaga O and Kahr B 2019 Mueller matrix polarimetry of bianisotropic materials *J. Opt. Soc. Am.* B **36** F72–F83
[107] Ghim Y S and Rhee H G 2019 Instantaneous thickness measurement of multilayer films by single-shot angle-resolved spectral reflectometry *Opt. Lett.* **44** 5418–21
[108] Choi G, Kim M, Kim J and Pahk H J 2020 Angle-resolved spectral reflectometry with a digital light processing projector *Opt. Express* **28** 26908–21
[109] Peng L H, Tang D W, Wang J, Chen R, Gao F and Zhou L P 2021 Robust incident angle calibration of angle-resolved ellipsometry for thin film measurement *Appl. Opt.* **60** 3971–6
[110] Oviroh P O, Akbarzadeh R, Pan D Q, Coetzee R A M and Jen T C 2019 New development of atomic layer deposition: processes, methods and applications *Sci. Technol. Adv. Mater.* **20** 465–96
[111] Cremers V, Puurunen R L and Dendooven J 2019 Conformality in atomic layer deposition: current status overview of analysis and modelling *Appl. Phys. Rev.* **6** 021302
[112] Nguyen V H, Sekkat A, Jiménez C, Muñoz D, Bellet D and Muñoz-Rojas D 2021 Impact of precursor exposure on process efficiency and film properties in spatial atomic layer deposition *Chem. Eng. J.* **403** 126234
[113] Li Z S, Xiang J R, Liu X, Li X B, Li L J, Shan B and Chen R 2022 A combined multiscale modeling and experimental study on surface modification of high-volume micro-nanoparticles with atomic accuracy *Int. J. Extreme Manuf.* **4** 025101
[114] Duan C L, Liu X, Shan B and Chen R 2015 Fluidized bed coupled rotary reactor for nanoparticles coating via atomic layer deposition *Rev. Sci. Instrum.* **86** 075101
[115] Gu H *et al* 2022 Modeling of deposit formation in mesoporous substrates via atomic layer deposition: insights from pore-scale simulation *AIChE J.* **68** e17889
[116] Cao K, Hu Q, Cai J M, Gong M, Yang J F, Shan B and Chen R 2018 Development of a scanning probe microscopy integrated atomic layer deposition system for in situ successive monitoring of thin film growth *Rev. Sci. Instrum.* **89** 123702
[117] Huang B, Yang W J, Wen Y W, Shan B and Chen R 2015 Co_3O_4-modified TiO_2 nanotube arrays via atomic layer

deposition for improved visible-light photoelectrochemical performance *ACS Appl. Mater. Interfaces* **7** 422–31
[118] Muñoz-Rojas D, Maindron T, Esteve A, Piallat F, Kools J C S and Decams J M 2019 Speeding up the unique assets of atomic layer deposition *Mater. Today Chem.* **12** 96–120
[119] Muñoz-Rojas D and MacManus-Driscoll J 2014 Spatial atmospheric atomic layer deposition: a new laboratory and industrial tool for low-cost photovoltaics *Mater. Horiz.* **1** 314–20
[120] Wang X L, Li Y, Lin J L, Shan B and Chen R 2017 Modular injector integrated linear apparatus with motion profile optimization for spatial atomic layer deposition *Rev. Sci. Instrum.* **88** 115108
[121] Deng Z, He W J, Duan C L, Chen R and Shan B 2016 Mechanistic modeling study on process optimization and precursor utilization with atmospheric spatial atomic layer deposition *J Vac. Sci. Technol.* A **34** 01A108
[122] Pan D Q 2019 Numerical study on the effectiveness of precursor isolation using N_2 as gas barrier in spatial atomic layer deposition *Int. J. Heat Mass Transfer* **144** 118642